Can the diphoton enhancement at 750 GeV be due to a neutral technipion?

Piotr Lebiedowicz,[1,*] Marta Łuszczak,[2,†] Roman Pasechnik,[3,‡] and Antoni Szczurek[1,§]

[1]*Institute of Nuclear Physics, Polish Academy of Sciences, PL-31-342 Kraków, Poland*
[2]*Department of Theoretical Physics, University of Rzeszów, PL-35-959 Rzeszów, Poland*
[3]*Department of Astronomy and Theoretical Physics, Lund University, SE-223 62 Lund, Sweden*

(Received 19 April 2016; published 19 July 2016)

We discuss a scenario in which the diphoton enhancement at $M_{\gamma\gamma} = 750$ GeV, observed by the ATLAS and CMS collaborations, is a neutral technipion $\tilde{\pi}^0$. We consider two distinct minimal models for the dynamical electroweak symmetry breaking. In a first one, two-flavor vectorlike technicolor (VTC) model, we assume that the two-photon fusion is a dominant production mechanism. We include $\gamma\gamma \to \tilde{\pi}^0$ and production of technipion associated with one or two jets. All the considered mechanisms give similar contributions. With the strong Yukawa (technipion-techniquark) coupling $g_{\rm TC} \simeq 20$ we roughly obtain the measured cross section of the "signal" with a small difficulty of simultaneous description of the $\sqrt{s} = 13$ TeV and $\sqrt{s} = 8$ TeV data. With such values of $g_{\rm TC}$ we get a relatively small $\Gamma_{\rm tot}$. In a second approach, one-family walking technicolor (WTC) model, the isoscalar technipion is produced dominantly via the gluon-gluon fusion. We also discuss the size of the signal at lower energies (LHC, Tevatron) for $\gamma\gamma$ (VTC) and jet-jet (WTC) final states and check consistency with the existing experimental data. We predict a measurable cross section for $\tilde{\pi}^0$ production associated with one or two soft jets. The technipion signal in both models is compared with the SM background diphoton contributions. We observe the dominance of the inelastic-inelastic mechanism for $\gamma\gamma$ induced processes. In the VTC scenario, we predict the signal cross section for purely exclusive $pp \to pp\gamma\gamma$ processes at $\sqrt{s} = 13$ TeV to be about 0.2 fb. Such a cross section would be, however, difficult to measure with the planned integrated luminosity. In all considered cases the signal is below the background or/and below the threshold set by statistics.

DOI: 10.1103/PhysRevD.94.015023

I. INTRODUCTION

Recently both the ATLAS and CMS collaborations announced an observation of an intriguing enhancement in the diphoton invariant mass at $M_{\gamma\gamma} \approx 750$ GeV in proton-proton collisions at $\sqrt{s} = 13$ TeV [1–4].[1] Remarkably, such a hint to a possible New Physics signal has triggered a lot of research activities in recent months looking for its possible interpretation in various theoretical scenarios of New Physics (see, e.g., Refs. [6–18]). However, before one could be certain about a possible nature of such a hint, it requires further confirmation by collecting a better statistics. If it is confirmed it will be a very important discovery related to first observation of the signal beyond Standard Model (SM). Different scenarios are possible *a priori*. The resonance signal observed means that the potentially new state decays into (and thus should couple to) two photons. What is the dominant production mechanism is a speculation at this stage. Several options are possible *a priori*. In one of them gluon-gluon fusion is the dominant production mechanism. If coupling of the new state to gluons is weak other options have to be considered. In the present analysis we consider such an example. The two-photon induced production of various objects became recently rather topical. This includes, for instance, production of $c\bar{c}$ [19], $b\bar{b}$ [20,21], l^+l^- [22,23], W^+W^- [24,25] or H^+H^- [26]. In the current study, we continue this line of research and consider the two-photon production mechanism of a new lightest composite state, the technipion predicted by various technicolor models, thus probing its potential to explain the 750 GeV excess.

A high-scale strongly coupled physics can, in principle, be responsible for the dynamical electroweak symmetry breaking (EWSB) in the SM by means of strongly interacting technifermion condensation (see e.g. Refs. [27–29]). Such a dynamics typically predicts plenty of new composite states close to the EWSB scale, in particular, relatively light composite scalar Higgs-like particles and pseudoscalar technipions. A consistent realization of the underlined compositeness scenarios is typically limited by the precision SM tests [30–32] and the ongoing SM-like Higgs boson studies [33] (for a detailed review see e.g. Refs. [34,35]). One of the appealing and consistent classes of the technicolor (TC) models with a vectorlike (Dirac) UV completion is known as the vectorlike TC (VTC) scenario [36]. The simplest version of the VTC scenario applied to the EWSB possessed two Dirac techniflavors and a SM-like Higgs

*Piotr.Lebiedowicz@ifj.edu.pl
†luszczak@univ.rzeszow.pl
‡Roman.Pasechnik@thep.lu.se
§Antoni.Szczurek@ifj.edu.pl
Also at University of Rzeszów, PL-35-959 Rzeszów, Poland.

[1]For a search of diphoton resonances at smaller mass range $65 < M_{\gamma\gamma} < 600$ GeV and $\sqrt{s} = 8$ TeV, see Ref. [5].

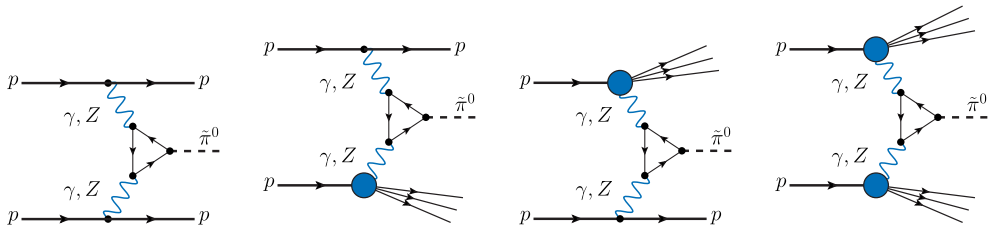

FIG. 1. Diagrams of neutral technipion production via the $\gamma\gamma$, γZ and ZZ fusion in pp-collisions.

boson [37–39]. Recently, the concept of Dirac UV completion has also emerged in composite Higgs boson scenarios with confined $SU(2)_{\rm TC}$ symmetry [40,41].

Below, we discuss possible implications of the neutral pseudoscalar technipion in the two-flavor VTC [37] and one-family walking TC (WTC) [42] scenarios of the dynamical EWSB for the diphoton 750 GeV signature at the LHC. In the simplest VTC scenario, the technipion does not couple to quarks and gluons and is thus produced only via the EW vector (γ and Z) boson fusion (VBF) mechanism with a slight dominance of the $\gamma\gamma$ fusion channel at large invariant masses. The corresponding technipion production processes can be classified into three groups depending on the QED order. The first group of diagrams is shown in Fig. 1. Diagrams in Fig. 2 show the higher QED-order group, that is, the technipion production associated with one jet. We consider here the $\gamma q \to \tilde{\pi}^0 q$ and $q\gamma \to \tilde{\pi}^0 q$ subprocesses. In even higher QED order we have to include also $q_i q_j' \to q_i \tilde{\pi}^0 q_j'$ subprocesses (see Fig. 3), where q_i and q_j can be either a quark or an antiquark of various flavors from each of the colliding protons. In the walking TC scenario, the technipion is produced dominantly by the ordinary gluon-gluon fusion (relevant also for the Higgs boson production at the LHC) and can decay with a sizable branching fraction into the two-photon final state. Other distinct scenarios were explored recently in Refs. [43–45] and will not be discussed here.

II. VECTORLIKE TC MODEL: A SHORT OVERVIEW

Before we go to the production mechanisms relevant for the neutral technipion production, let us summarize the main points of the VTC model.

The Dirac techniquarks in the minimal two-flavor VTC model form pseudoreal representations of the global $SU(4)$ group which contains the chiral $SU(2)_L \otimes SU(2)_R$ symmetry in the technimeson sector. In the linear realization of the VTC model, at low energies the global chiral $SU(2)_L \otimes SU(2)_R$ symmetry describes the effective interactions the lightest technimeson states, technipion P^a ($a = 1, 2, 3$), technisigma S and constituent Dirac techniquarks $\tilde{Q}_\alpha$ $\alpha = 1, 2$ [37,39], similar to those in quark-meson effective theories of QCD hadron physics [46].

For the Dirac UV completion, the vector subgroup of the global chiral group $SU(2)_{V\equiv L+R}$ and the local weak-isospin symmetry of the SM $SU(2)_W$ are locally isomorphic. Therefore, the representations of the $SU(2)_V$ can always be mapped onto the representations of $SU(2)_W$ such that the P^a, S and Dirac $\tilde{Q}_\alpha$ can be classified as triplet, singlet and doublet representations of the gauge $SU(2)_W$ symmetry. Such a straightforward way of introducing weak interactions into the technimeson sector was proposed in the framework of the VTC model in Ref. [37]. In particular, it was demonstrated for the first time that practically any simple Dirac UV completion with chirally symmetric weak interactions naturally escapes the electroweak precision constraints which is considered the basic motivation for the VTC scenario despite its simplicity.

Let us consider a single $SU(2)_{\rm W}$ doublet of Dirac techniquarks,

$$\tilde{Q} = \begin{pmatrix} U \\ D \end{pmatrix}, \tag{2.1}$$

confined under $SU(N_{\rm TC})_{\rm TC}$ at an energy scale $\Lambda_{\rm TC}$ above the EW scale. For a QCD-like scenario we choose $N_{\rm TC} = 3$ and the hypercharge $Y_{\tilde{Q}} = 1/3$ provided that electric

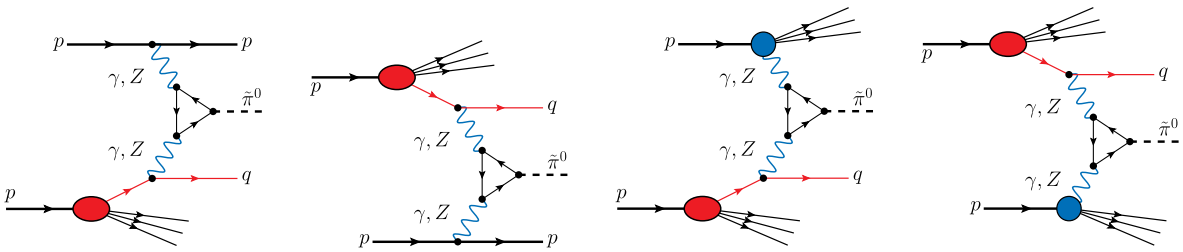

FIG. 2. Technipion production via the $2 \to 2$ partonic subprocesses.

charges of corresponding bounds states are integer valued. Then, the phenomenological interactions of the constituent techniquarks and the lightest technimesons are described by the (global) chiral $SU(2)_{\rm R} \otimes SU(2)_{\rm L}$ invariant low-energy effective Lagrangian in the linear σ-model (LσM),

$$\begin{aligned}\mathcal{L}_{\rm L\sigma M} &= \frac{1}{2}\partial_\mu S \partial^\mu S + \frac{1}{2} D_\mu P_a D^\mu P_a + i\bar{\tilde{Q}}\hat{D}\tilde{Q} \\ &\quad - g_{\rm TC}\bar{\tilde{Q}}(S + i\gamma_5 \tau_a P_a)\tilde{Q} - g_{\rm TC} S\langle\bar{\tilde{Q}}\tilde{Q}\rangle \\ &\quad - \lambda_{\rm H}\mathcal{H}^4 - \frac{1}{4}\lambda_{\rm TC}(S^2+P^2)^2 + \lambda\mathcal{H}^2(S^2+P^2) \\ &\quad + \frac{1}{2}\mu_{\rm S}^2(S^2+P^2) + \mu_{\rm H}^2\mathcal{H}^2, \end{aligned} \tag{2.2}$$

where the "source" term linear in technisigma is proportional to the flavor-diagonal techniquark condensate $\langle\bar{\tilde{Q}}\tilde{Q}\rangle < 0$, $\mathcal{H}^2 = \mathcal{H}\mathcal{H}^\dagger$, $P^2 \equiv P_a P_a = \tilde{\pi}^0\tilde{\pi}^0 + 2\tilde{\pi}^+\tilde{\pi}^-$, and the corresponding covariant derivatives read

$$\begin{aligned}\hat{D}\tilde{Q} &= \gamma^\mu\left(\partial_\mu - \frac{iY_{\tilde{Q}}}{2}g' B_\mu - \frac{i}{2}g W_\mu^a \tau_a\right)\tilde{Q}, \\ D_\mu P_a &= \partial_\mu P_a + g\epsilon_{abc} W_\mu^b P_c. \end{aligned} \tag{2.3}$$

For simplicity, the Higgs boson doublet $\mathcal{H}$ is kept to be elementary. The choice of the source term in Eq. (2.2) is rather natural since it (a) induces a pseudo-Goldstone mass scale for pseudo-Goldstone technipion $m_{\tilde{\pi}}$, and (b) relates the scales of the spontaneous EW and chiral symmetry breakings as well as the constituent techniquark mass scale $m_{\tilde{Q}}$ with the value of the techniquark condensate [37,46].

In the conformal limit of the theory $\mu_{S,H} \ll m_{\tilde{\pi}}$, the EW and chiral symmetries are broken by the Higgs $v \simeq 246$ GeV and technisigma u vevs

$$\begin{aligned}&\mathcal{H} = \frac{1}{\sqrt{2}}\begin{pmatrix}\sqrt{2}i\phi^- \\ H + i\phi^0\end{pmatrix}, \qquad \langle H\rangle \equiv v, \qquad \langle S\rangle \equiv u \gtrsim v, \\ &H = v + hc_\theta - \tilde{\sigma}s_\theta, \qquad S = u + hs_\theta + \tilde{\sigma}c_\theta, \end{aligned} \tag{2.4}$$

respectively, which are initiated by the techniquark condensation in the confined regime, i.e.

$$\begin{aligned}u &= \left(\frac{g_{\rm TC}\lambda_{\rm H}}{\delta}\right)^{1/3}|\langle\bar{\tilde{Q}}\tilde{Q}\rangle|^{1/3}, \\ v &= \left(\frac{|\lambda|}{\lambda_{\rm H}}\right)^{1/2}\left(\frac{g_{\rm TC}\lambda_{\rm H}}{\delta}\right)^{1/3}|\langle\bar{\tilde{Q}}\tilde{Q}\rangle|^{1/3}. \end{aligned} \tag{2.5}$$

Then, technipions and techniquarks acquire a dynamical effective mass

$$\begin{aligned}m_\pi^2 &= -\frac{g_{\rm TC}\langle\bar{\tilde{Q}}\tilde{Q}\rangle}{u}, \\ m_U &= m_D \equiv m_{\tilde{Q}} = g_{\rm TC} u. \end{aligned}$$

Above, $s_\theta \equiv \sin\theta$, $c_\theta \equiv \cos\theta$, $\delta = \lambda_{\rm H}\lambda_{\rm TC} - \lambda^2$, $g_{\rm TC} > 0$ and $\lambda_H > 0$. The phenomenologically consistent regime corresponds to a small Higgs-technisigma mixing $\theta \ll 1$ which is realized in the TC decoupling limit $v/u \ll 1$ [37]. As a characteristic feature of the model, the technipions in the VTC model can stay relatively light and do not have tree-level couplings to the SM fermions, so can only be produced in vector-boson fusion channels [37,38]. In what follows, we discuss possible signatures of the VTC technipions at the LHC.

A. Decay widths for the neutral technipion in the vectorlike TC model

The techniquark-loop amplitude has the following form [37]:

$$i\mathcal{V}_{\tilde{\pi}^0 V_1 V_2} = F_{V_1V_2}(m_1^2, m_2^2, m_{\tilde{\pi}^0}^2; m_{\tilde{Q}}^2)\epsilon_{\mu\nu\rho\sigma}p_1^\mu p_2^\nu \varepsilon_1^{*\rho}\varepsilon_2^{*\sigma}, \tag{2.6}$$

$$F_{V_1V_2} = \frac{N_{\rm TC}}{2\pi^2}\sum_{\tilde{Q}=U,D} g_{V_1}^{\tilde{Q}} g_{V_2}^{\tilde{Q}} g_{\tilde{\pi}^0}^{\tilde{Q}} m_{\tilde{Q}} C_0(m_1^2, m_2^2, m_{\tilde{\pi}}^2; m_{\tilde{Q}}^2), \tag{2.7}$$

where $C_0(m_1^2, m_2^2, m_3^2; m^2) \equiv C_0(m_1^2, m_2^2, m_3^2; m^2, m^2, m^2)$ is the standard finite three-point function, $p_{1,2}$, $\varepsilon_{1,2}$ and $M_{1,2}$ are the four-momenta, polarization vectors of the vector bosons $V_{1,2}$ and their on-shell masses, respectively, and neutral technipion couplings to U, D techniquarks are

$$g_{\tilde{\pi}^0}^U = g_{\rm TC}, \qquad g_{\tilde{\pi}^0}^D = -g_{\rm TC}, \tag{2.8}$$

while gauge couplings of techniquarks $g_{V_{1,2}}^{\tilde{Q}}$ are defined in Ref. [37]. Finally, the explicit expressions of the effective neutral technipion couplings $F_{V_1V_2}$ for on-shell $V_1V_2 = \gamma\gamma$, γZ and ZZ final states are[2]

$$F_{\gamma\gamma} = \frac{4\alpha_{\rm em} g_{\rm TC}}{\pi}\frac{m_{\tilde{Q}}}{m_{\tilde{\pi}^0}^2}\arcsin^2\left(\frac{m_{\tilde{\pi}^0}}{2m_{\tilde{Q}}}\right), \quad \frac{m_{\tilde{\pi}^0}}{2m_{\tilde{Q}}} < 1, \tag{2.9}$$

$$\begin{aligned}F_{\gamma Z} = \frac{4\alpha_{\rm em} g_{\rm TC}}{\pi}\frac{m_{\tilde{Q}}}{m_{\tilde{\pi}^0}^2}\cot 2\theta_W \Bigg[&\arcsin^2\left(\frac{m_{\tilde{\pi}^0}}{2m_{\tilde{Q}}}\right) \\ &- \arcsin^2\left(\frac{m_Z}{2m_{\tilde{Q}}}\right)\Bigg], \end{aligned} \tag{2.10}$$

$$F_{ZZ} = \frac{2\alpha_{\rm em} g_{\rm TC}}{\pi} m_{\tilde{Q}} C_0(m_Z^2, m_Z^2, m_{\tilde{\pi}^0}^2; m_{\tilde{Q}}^2), \tag{2.11}$$

where $\alpha_{\rm em} = e^2/(4\pi)$ is the fine structure constant.

[2]We should notice here that the $\tilde{\pi}^0 \to W^+W^-$ decay mode is forbidden by symmetry [37].

Now the two-body technipion decay width in a vector boson channel can be represented in terms of the effective couplings (2.7) as follows:

$$\Gamma(\tilde{\pi}^0 \to V_1 V_2) = r_V \frac{m_{\tilde{\pi}}^3}{64\pi} \bar{\lambda}^3(m_1, m_2; m_{\tilde{\pi}}) |F_{V_1 V_2}|^2, \quad (2.12)$$

where $r_V = 1$ for identical bosons V_1 and V_2 and $r_V = 2$ for different ones, and $\bar{\lambda}$ is the normalized Källén function,

$$\bar{\lambda}(m_a, m_b; q) = \left(1 - 2\frac{m_a^2 + m_b^2}{q^2} + \frac{(m_a^2 - m_b^2)^2}{q^4}\right)^{1/2}. \quad (2.13)$$

For example, in the VTC model, for $g_{\rm TC} = 10$ and $m_{\tilde{Q}} = 0.75 m_{\tilde{\pi}^0}$ one gets:

$$\Gamma(\tilde{\pi}^0 \to \gamma\gamma) = 5.136 \times 10^{-3}\ \text{GeV}, \quad (2.14)$$

$$\Gamma(\tilde{\pi}^0 \to \gamma Z) = 4.376 \times 10^{-3}\ \text{GeV}, \quad (2.15)$$

$$\Gamma(\tilde{\pi}^0 \to ZZ) = 4.734 \times 10^{-3}\ \text{GeV}. \quad (2.16)$$

The total decay width is a sum of the tree contributions:

$$\Gamma_{\rm tot} = \Gamma(\tilde{\pi}^0 \to \gamma\gamma) + \Gamma(\tilde{\pi}^0 \to \gamma Z) + \Gamma(\tilde{\pi}^0 \to ZZ). \quad (2.17)$$

The corresponding branching fractions are

$$\text{Br}(\tilde{\pi}^0 \to \gamma\gamma) = 0.36, \quad (2.18)$$

$$\text{Br}(\tilde{\pi}^0 \to \gamma Z) = 0.31, \quad (2.19)$$

$$\text{Br}(\tilde{\pi}^0 \to ZZ) = 0.33. \quad (2.20)$$

How the total decay width depends on the model coupling constant $g_{\rm TC}$ is shown in Fig. 4. Only at very large $g_{\rm TC} =$ 300–400 one can reproduce the ATLAS quasiexperimental value $\Gamma_{\rm tot} \simeq 45$ GeV [3,4] (only the ATLAS collaboration claims that the observed state is broad). Such a gigantic value is far too big compared to an analogical coupling in effective quark-hadron interactions in low-energy QCD such that the model loses its physical sense. However, the extraction of the total width from the "experimental data" is highly speculative and biased and thus should not be taken too seriously.

III. PRODUCTION MECHANISMS OF NEUTRAL TECHNIPION

As mentioned in the Introduction we shall consider contributions of different QED orders to the production of hypothetical technipions as shown in Figs. 1–3. Let us briefly discuss all the contributions one by one.

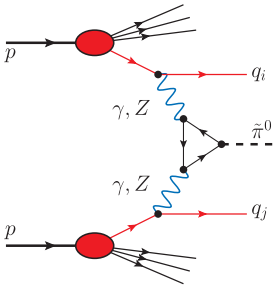

FIG. 3. Technipion production via the $2 \to 3$ partonic subprocesses.

As already discussed above in our VTC model [37] the technipion couples only to photons and Z bosons. In the present paper, we shall include only coupling to photons as far as the production mechanism of technipion is considered. The couplings to Z bosons do not affect the observables significantly and will be considered elsewhere.

A. $2 \to 1$ subprocess

The corresponding diagrams in Fig. 1 can be categorized into three groups (elastic-elastic, elastic-inelastic, inelastic-inelastic) depending on whether the protons survive intact or undergo electromagnetic dissociation.

The cross section for the $2 \to 1$ contribution via the subprocess $\gamma\gamma \to \tilde{\pi}^0$ can be easily written in the compact form:

$$\frac{d\sigma_{pp\to\tilde{\pi}^0}}{dy_{\tilde{\pi}^0}} = \frac{\pi}{m_{\tilde{\pi}^0}^4} \sum_{i,j} x_1\gamma^{(i)}(x_1, \mu_F^2) x_2\gamma^{(j)}(x_2, \mu_F^2) \overline{|\mathcal{M}_{\gamma\gamma\to\tilde{\pi}^0}|^2}, \quad (3.1)$$

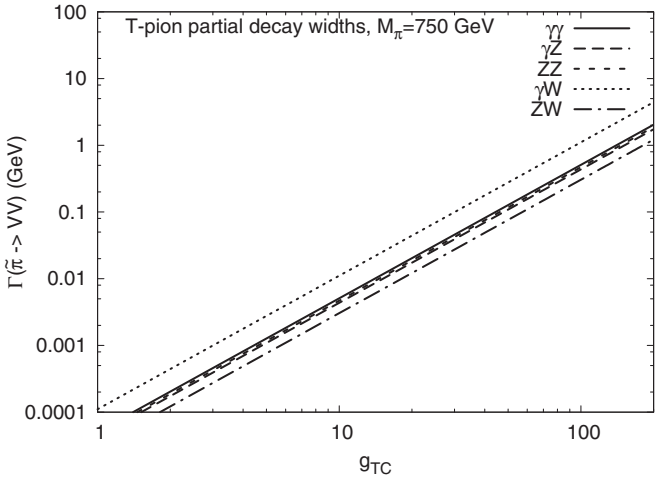

FIG. 4. Decay width in GeV as a function of $g_{\rm TC}$ coupling constant. The γW and ZW final states are only for charged technipions. Here we have used our benchmark choice $m_{\tilde{Q}} = 0.75 m_{\tilde{\pi}}$.

where indices i and j denote $i,j = \mathrm{el}$ or in, i.e. they correspond to elastic or inelastic flux (x-distribution) of equivalent photons, respectively, and x_1, x_2 are the longitudinal momentum fractions of the proton

$$x_1 = \frac{m_{\tilde{\pi}^0}}{\sqrt{s}}\exp(y_{\tilde{\pi}^0}), \qquad x_2 = \frac{m_{\tilde{\pi}^0}}{\sqrt{s}}\exp(-y_{\tilde{\pi}^0}), \tag{3.2}$$

where $y_{\tilde{\pi}^0}$ is rapidity of the technipion. The elastic photon fluxes are calculated using the Drees-Zeppenfeld parametrization [47,48], where a simple parametrization of the nucleon electromagnetic form factors is used. To calculate inelastic contributions we use the collinear approach with photon MRST(QED) PDFs [49]. In formula (3.1) the μ_F^2 factorization scale makes sense only in the case of dissociation of a proton. Here we take $\mu_F^2 = m_{\tilde{\pi}^0}^2$. In the leading-order collinear approximation the technipion is produced with zero transverse momentum. The matrix element squared has been calculated with an effective $\gamma\gamma \to \tilde{\pi}^0$ vertex. In general, the form factor (2.9) describes the coupling of two photons to the technipion resonance could depend on virtualities of photons.

B. $2 \to 2$ subprocess

Now we discuss diagrams shown in Fig. 2 with the $\gamma q \to \tilde{\pi}^0 q$ and $q\gamma \to \tilde{\pi}^0 q$ subprocesses. The cross section can be also written in a compact way which allows easy calculation of differential distributions:

$$\begin{aligned}\frac{d\sigma}{dy_3 dy_4 d^2p_{t,\tilde{\pi}^0}} &= \frac{1}{16\pi^2\hat{s}^2}\sum_i x_1\gamma^{(i)}(x_1,\mu_F^2)x_2 q_{\mathrm{eff}}(x_2,\mu_F^2)\overline{|\mathcal{M}_{\gamma q\to\tilde{\pi}^0 q}|^2} \\ &+ \frac{1}{16\pi^2\hat{s}^2}\sum_j x_1 q_{\mathrm{eff}}(x_1,\mu_F^2)x_2\gamma^{(j)}(x_2,\mu_F^2)\overline{|\mathcal{M}_{q\gamma\to\tilde{\pi}^0 q}|^2},\end{aligned} \tag{3.3}$$

where index "3" refers to technipion and index "4" refers to outgoing quark/antiquark and

$$\begin{aligned} x_1 &= \frac{m_{1\perp}}{\sqrt{s}}\exp(y_3) + \frac{m_{2\perp}}{\sqrt{s}}\exp(y_4), \\ x_2 &= \frac{m_{1\perp}}{\sqrt{s}}\exp(-y_3) + \frac{m_{2\perp}}{\sqrt{s}}\exp(-y_4), \\ m_{1\perp} &= \sqrt{m_{\tilde{\pi}^0}^2 + p_{t,\tilde{\pi}^0}^2}, \\ m_{2\perp} &= p_{t,\tilde{\pi}^0}. \end{aligned} \tag{3.4}$$

In this approach, transverse momenta of $\tilde{\pi}^0$ and outgoing $q/\bar{q}$ are strictly balanced. Here we have introduced effective parton distribution which we define as

$$q_{\mathrm{eff}}(x,\mu^2) = \sum_f e_f^2(q_f(x,\mu^2) + \bar{q}_f(x,\mu^2)), \tag{3.5}$$

where we take $\mu^2 = p_{t,\tilde{\pi}^0}^2$. The matrix element for the $\gamma q \to \tilde{\pi}^0 q$ process reads

$$\begin{aligned}\mathcal{M}_{\gamma q\to\tilde{\pi}^0 q} &= F_{\gamma\gamma}\varepsilon^{\mu\nu\kappa\alpha}p_{1\mu}p_{3\nu}\varepsilon_\kappa^{(\gamma)}(p_1,\lambda_1) \\ &\times\frac{-ig_{\alpha\beta}}{k^2}\bar{u}(p_4,\lambda_4)\gamma^\beta u(p_2,\lambda_2),\end{aligned} \tag{3.6}$$

where $k^2 = (p_2 - p_4)^2 = (p_1 - p_3)^2$. The matrix element squared including masses of quarks can be written in terms of the Mandelstam variables as

$$\begin{aligned}\overline{|\mathcal{M}_{\gamma q\to\tilde{\pi}^0 q}|^2} &= \frac{1}{4}F_{\gamma\gamma}^2\frac{2e^2}{\hat{t}^2}[2(\hat{s}-m_q^2)(k\cdot p_1)(k\cdot p_4) \\ &+ 2(m_q^2-\hat{u})(k\cdot p_1)(k\cdot p_2) - 4m_q^2(k\cdot p_1)^2 \\ &+ \hat{t}(m_q^2-\hat{s})(m_q^2-\hat{u})],\end{aligned} \tag{3.7}$$

$$\begin{aligned}\overline{|\mathcal{M}_{q\gamma\to\tilde{\pi}^0 q}|^2} &= \frac{1}{4}F_{\gamma\gamma}^2\frac{2e^2}{\hat{t}^2}[2(\hat{s}-m_q^2)(k\cdot p_2)(k\cdot p_4) \\ &+ 2(m_q^2-\hat{u})(k\cdot p_2)(k\cdot p_1) - 4m_q^2(k\cdot p_2)^2 \\ &+ \hat{t}(m_q^2-\hat{s})(m_q^2-\hat{u})].\end{aligned} \tag{3.8}$$

C. $2 \to 3$ subprocess

As the last contribution we discuss the diagram in Fig. 3. The cross section for the partonic $qq' \to q\tilde{\pi}^0 q'$ process can be written as

$$\sigma_{qq'\to q\tilde{\pi}^0 q'} = \frac{1}{2\hat{s}}\overline{|\mathcal{M}_{qq'\to q\tilde{\pi}^0 q'}|^2}\mathcal{J}d\xi_1 d\xi_2 dy_{\tilde{\pi}^0}d\phi_{12}, \tag{3.9}$$

where ϕ_{12} is the relative azimuthal angle between q and q', $\xi_1 = \log_{10}(p_{1t}/1\ \mathrm{GeV})$ and $\xi_2 = \log_{10}(p_{2t}/1\ \mathrm{GeV})$, where p_{1t} and p_{2t} are transverse momenta of outgoing q and q', respectively. The matrix element was calculated as[3]

$$\begin{aligned}&\mathcal{M}_{qq'\to q\tilde{\pi}^0 q'}(\lambda_1,\lambda_2,\lambda_3,\lambda_4) \\ &= e^2\bar{u}(p_3,\lambda_3)\gamma^\mu u(p_1,\lambda_1)\frac{-ig_{\mu\nu}}{\hat{t}_1} \\ &\times\varepsilon^{\nu\nu'\alpha\beta}q_{1\alpha}q_{2\beta}F_{\gamma\gamma}\frac{-ig_{\nu'\mu'}}{\hat{t}_2}\bar{u}(p_4,\lambda_4)\gamma^{\mu'}u(p_2,\lambda_2).\end{aligned} \tag{3.10}$$

For comparison, we shall also calculate the matrix element in the high-energy approximation:

[3]We have also obtained a formula for matrix element squared by using the MATHEMATICA package FEYNCALC [50,51] and checked that it gives the same result as the calculation with explicit use of spinors.

$$\bar{u}(p',\lambda')\gamma^\mu u(p,\lambda) \to (p'+p)^\mu \delta_{\lambda'\lambda}, \tag{3.11}$$

often used in the literature in a different context, see e.g. [26].

The total (phase-space integrated) cross section for technipion production could be alternatively calculated as

$$\sigma_{pp\to\tilde{\pi}^0 jj} = \int dx_1 dx_2 \sum_{f_1,f_2} q_{f_1}(x_1,\mu_F^2) \times q_{f_2}(x_2,\mu_F^2)\hat{\sigma}_{f_1 f_2\to f_1\tilde{\pi}^0 f_2}(\hat{s}). \tag{3.12}$$

Limiting to $\gamma\gamma$-fusion processes only one can write

$$\sigma^{\gamma\gamma}_{pp\to\tilde{\pi}^0 jj} = \int dx_1 dx_2 q_{\rm eff}(x_1,\mu_F^2) \times q_{\rm eff}(x_2,\mu_F^2)\hat{\sigma}^{\rm eff}_{qq\to q\tilde{\pi}^0 q}(\hat{s}), \tag{3.13}$$

where $\hat{\sigma}^{\rm eff}_{qq\to q\tilde{\pi}^0 q}(\hat{s})$ is then the integrated cross section for the $f_1 f_2 \to f_1\tilde{\pi}^0 f_2$ subprocess with both fractional quark/antiquark charges set to unity.

The above formula (3.12) is not very efficient when calculating subprocess energy distribution. A more useful formula is

$$\sigma_{pp\to\tilde{\pi}^0 jj} = \int dW \left(\hat{\sigma}^{\rm eff}_{qq\to q\tilde{\pi}^0 q}(W) \times \int dx_d (\mathcal{J} q_{\rm eff}(x_1,\mu_F^2) q_{\rm eff}(x_2,\mu_F^2)) \right). \tag{3.14}$$

Above $W=\sqrt{\hat{s}}$, $x_d = x_1 - x_2$, and $\mathcal{J}$ is a Jacobian of the transformation from (x_1, x_2) to (W, x_d). In practical calculation, the first partonic $\hat{\sigma}^{\rm eff}_{qq'\to q\tilde{\pi}^0 q'}$ (assuming elementary charges of quarks/antiquarks) is calculated as a function of W on a grid and then the convolution with parton distributions is done as shown in Eq. (3.14). In the $2\to 3$ hadronic calculations we take $\mu_F^2 = m^2_{\tilde{\pi}^0}$.

IV. LEADING ORDER VTC TECHNIPION SIGNAL IN THE DIPHOTON CHANNEL

In the case of the VTC technipion model [37], the amplitude for the $\gamma\gamma\to\tilde{\pi}^0\to\gamma\gamma$ subprocess reads

$$\begin{aligned}\mathcal{M}_{\gamma\gamma\to\tilde{\pi}^0\to\gamma\gamma}(\lambda_1,\lambda_2,\lambda_3,\lambda_4) &= (\varepsilon^{(\gamma)\mu_3}(p_3,\lambda_3))^*(\varepsilon^{(\gamma)\mu_4}(p_4,\lambda_4))^* \\ &\times \epsilon_{\mu_3\mu_4\nu_3\nu_4} p_3^{\nu_3} p_4^{\nu_4} F_{\gamma\gamma} \frac{i}{\hat{s}-m^2_{\tilde{\pi}^0}+im_{\tilde{\pi}^0}\Gamma_{\rm tot}} \\ &\times \epsilon_{\mu_1\mu_2\nu_1\nu_2} p_1^{\nu_1} p_2^{\nu_2} F_{\gamma\gamma}\varepsilon^{(\gamma)\mu_1}(p_1,\lambda_1)\varepsilon^{(\gamma)\mu_2}(p_2,\lambda_2). \end{aligned}\tag{4.1}$$

The $\Gamma_{\rm tot}$ can be calculated from a model or taken from recent experimental data. In the following we take the calculated value of $\Gamma_{\rm tot}$ and $m_{\tilde{\pi}^0} = 750$ GeV. The mass scale of the degenerate techniquarks $m_{\tilde{Q}}$ is in principle another free parameter (see Ref. [38]).

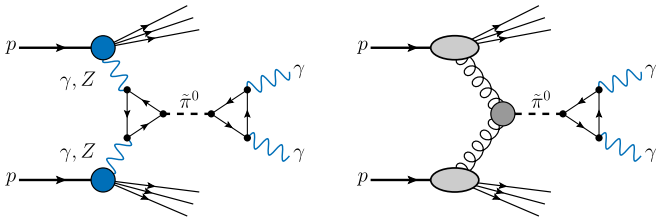

FIG. 5. Leading order technipion signal in the diphoton channel in proton-proton collisions.

The cross section for the signal (see the left panel of Fig. 5) is calculated as ($\mu_F^2 = p_{t,\gamma}^2$)

$$\frac{d\sigma}{dy_3 dy_4 d^2p_{t,\gamma}} = \frac{1}{16\pi^2\hat{s}^2}\sum_{i,j} x_1\gamma^{(i)}(x_1,\mu_F^2) x_2\gamma^{(j)} \times (x_2,\mu_F^2)\overline{|\mathcal{M}_{\gamma\gamma\to\tilde{\pi}^0\to\gamma\gamma}|^2}, \tag{4.2}$$

where

$$\begin{aligned} x_1 &= \frac{p_{t,\gamma}}{\sqrt{s}}[\exp(y_3)+\exp(y_4)], \\ x_2 &= \frac{p_{t,\gamma}}{\sqrt{s}}[\exp(-y_3)+\exp(-y_4)]. \end{aligned}\tag{4.3}$$

V. ONE-FAMILY WALKING TECHNICOLOR MODEL

In the one-family walking technipion model discussed recently in Ref. [42] (see also references therein) the partial gg and $\gamma\gamma$ decay widths are given as

$$\Gamma(P^0\to gg) = \frac{N_{\rm TC}^2\alpha_s^2 G_F m^3_{P^0}}{12\sqrt{2}\pi^3}, \tag{5.1}$$

$$\Gamma(P^0\to\gamma\gamma) = \frac{N_{\rm TC}^2\alpha_{\rm em}^2 G_F m^3_{P^0}}{54\sqrt{2}\pi^3}, \tag{5.2}$$

where $\alpha_s \equiv g_s^2/(4\pi)$ is the strong coupling constant, $N_{\rm TC}$ is the number of technicolors in the walking technicolor model. For $N_{\rm TC}=3$ we get

$$\Gamma(P^0\to gg) = 1.2\ \text{GeV}, \qquad \Gamma(P^0\to\gamma\gamma) = 1.2\ \text{MeV}.$$

The decay into two gluons is in this model the dominant decay channel [42]. The total decay width in the model is therefore also much smaller than the 45 GeV reported in Refs. [3,4] and used in many very recent analyses. We will return to this point in the result section. It is interesting that the model gives the roughly correct size of the signal for $N_{\rm TC}=3$, 4, without any additional tuning.

The cross section for the signal in this scenario is calculated then as ($\mu_F^2 = p_{t,\gamma}^2$)

$$\frac{d\sigma}{dy_3 dy_4 d^2p_{t,\gamma}} = \frac{1}{16\pi^2\hat{s}^2}\frac{1}{N_c^2-1} x_1 g(x_1,\mu_F^2) \times x_2 g(x_2,\mu_F^2)\overline{|\mathcal{M}_{gg\to\tilde{\pi}^0\to\gamma\gamma}|^2}. \quad (5.3)$$

The color factor N_c guarantees that the technipion resonance is a QCD-white object. Clearly, in this model the gluon-gluon fusion is the dominant reaction mechanisms. This would also mean a rather large cross section for the dijet production of the order of a few pb. We shall show below whether this is compatible with the existing data for dijet production.

VI. PRODUCTION MECHANISMS OF BACKGROUND IN THE $\gamma\gamma$ CHANNEL

In the present exploratory analysis we consider the background contributions shown in Fig. 6. These include the $q\bar{q}$ annihilation [diagram (a)], the gluon-gluon fusion via quark boxes [diagram (b)], and the photon-photon fusion via lepton, quark and W-boson loops [diagram (c)]. The $\gamma\gamma$ fusion was found to be very important for W^+W^- production at large $M_{W^+W^-}$ [25]. In addition, this type of background could interfere with the signal. For simplicity we shall neglect these interference effects in the present paper.

A. Background $q\bar{q}$ annihilation contribution

The lowest order process for diphoton production is quark-antiquark annihilation. The cross section for $q\bar{q}$ annihilation can be written as

$$\frac{d\sigma}{dy_3 dy_4 d^2p_{t,\gamma}} = \frac{1}{16\pi^2\hat{s}^2}\sum_f x_1 q_f(x_1,\mu_F^2) \times x_2 \bar{q}_f(x_2,\mu_F^2)\overline{|\mathcal{M}_{q\bar{q}\to\gamma\gamma}|^2}. \quad (6.1)$$

The formula for the matrix element squared for the $q\bar{q}\to\gamma\gamma$ subprocess can be found e.g. in Ref. [52]. In our calculation we include only three quark flavors (u, d, s).

B. Background gg fusion contribution

For a test and for a comparison we also consider the gluon-gluon contribution to the inclusive cross section. The photons produced in $pp(\bar{p})\to\gamma\gamma+X$ are expected to be dominantly produced by the quark-antiquark annihilation ($q\bar{q}\to\gamma\gamma$) and by the gluon-gluon fusion ($gg\to\gamma\gamma$) through a quark-box diagram. The latter process is important especially at low diphoton invariant masses in the kinematic region with high gluon luminosity.

In the lowest order of pQCD the formula for inclusive cross section can be written as

$$\frac{d\sigma}{dy_3 dy_4 d^2p_{t,\gamma}} = \frac{1}{16\pi^2\hat{s}^2} x_1 g(x_1,\mu_F^2) x_2 g(x_2,\mu_F^2)\overline{|\mathcal{M}_{gg\to\gamma\gamma}|^2}. \quad (6.2)$$

The corresponding matrix elements have been discussed in detail e.g. in Ref. [53].

C. Background $\gamma\gamma$ fusion contribution

The cross section of $\gamma\gamma$ production via $\gamma\gamma$ fusion in pp collisions can be calculated in the same way as in the parton model in the so-called equivalent photon approximation as

$$\frac{d\sigma}{dy_3 dy_4 d^2p_{t,\gamma}} = \frac{1}{16\pi^2\hat{s}^2}\sum_{i,j} x_1\gamma^{(i)}(x_1,\mu_F^2) \times x_2\gamma^{(j)}(x_2,\mu_F^2)\overline{|\mathcal{M}_{\gamma\gamma\to\gamma\gamma}|^2}. \quad (6.3)$$

The loop-induced helicity matrix element for the $\gamma\gamma\to\gamma\gamma$ subprocess was calculated by using the MATHEMATICA package FORMCALC [54] and the LOOPTOOLS library based on [55] to evaluate one-loop integrals. In numerical calculations we include the full set of SM contributions including quark, lepton and W boson loops. At high diphoton invariant masses $M_{\gamma\gamma} \gtrsim 200$ GeV the inclusion of diagrams with W bosons in loops is crucial, e.g. in context of exclusive diphoton background production, see Fig. 12 of [38].

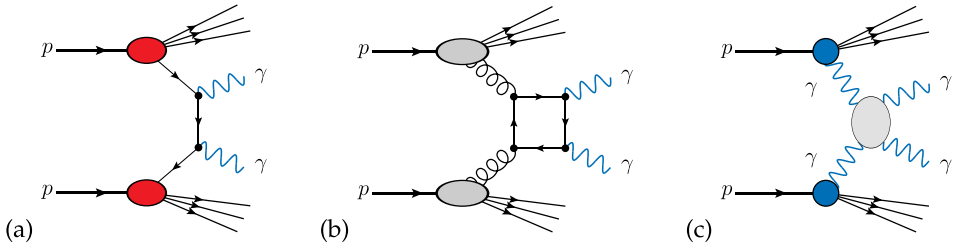

FIG. 6. Background mechanisms of $\gamma\gamma$ pairs production in proton-proton collisions.

TABLE I. Hadronic cross section in fb for neutral technipion production at $\sqrt{s} = 1.96$, 7, 8, 13, 100 TeV for different contributions shown in Figs. 1–3. Here we assume $g_{\rm TC} = 10$ and $m_{\tilde{Q}} = 0.75 m_{\tilde{\pi}^0}$. The total cross sections corresponding to the sum of all components for each type of partonic subprocesses are given in bold face.

Component	1.96 TeV	7 TeV	8 TeV	13 TeV	100 TeV
$2 \to 1$ (in, in)	1.37×10^{-3}	0.16	0.22	0.55	8.08
$2 \to 1$ (in, el)	0.22×10^{-3}	0.05	0.06	0.15	1.88
$2 \to 1$ (el, in)	0.22×10^{-3}	0.05	0.06	0.15	1.88
$2 \to 1$ (el, el)	0.03×10^{-3}	0.01	0.02	0.04	0.42
$2 \to 1$, sum of all	$\mathbf{1.84 \times 10^{-3}}$	**0.27**	**0.36**	**0.89**	**12.26**
$2 \to 2$ (in, in), two diagrams	0.74×10^{-3}	0.14	0.19	0.49	7.69
$2 \to 2$ (in, el) and (el, in)	0.13×10^{-3}	0.05	0.07	0.19	2.93
$2 \to 2$, sum of all	$\mathbf{0.87 \times 10^{-3}}$	**0.19**	**0.26**	**0.68**	**10.62**
$2 \to 2$, sum of all, $p_{t,\rm jet} > 10$ GeV				0.43	8.03
$2 \to 2$, sum of all, $p_{t,\rm jet} > 20$ GeV				0.35	6.99
$2 \to 2$, sum of all, $p_{t,\rm jet} > 50$ GeV				0.25	5.42
$2 \to 3$	$\mathbf{0.14 \times 10^{-3}}$	**0.09**	**0.13**	**0.46**	**16.71**
$2 \to 3$, $p_{t,\rm jet} > 10$ GeV				0.04	1.41

VII. DISCUSSION OF RESULTS AND CONSISTENCY CHECKS WITH EXISTING EXPERIMENTS

A. Signal of technipion

Let us first summarize integrated cross sections for the VTC scenario. In Table I we have collected cross sections for different QED orders. We neglect here intermediate Z exchanges for simplicity. For consistency all cross sections were calculated with the MRST(QED) PDFs [49]. In this calculation we have used $g_{\rm TC} = 10$ for example and our benchmark parameters. Surprisingly, different contributions are of the same order of magnitude. To describe the experimental signal more precisely $g_{\rm TC}$ can be rescaled. The result consistent with the cross sections for the signal extracted very recently from experimental ATLAS and/or CMS data is obtained with $g_{\rm TC} \simeq 20$ as will be shown at the end of this section.

We shall discuss now some specific results for different processes.

Let us start from the signal in the VTC model [37]. In this $(2 \to 1)$ calculation the $\sigma^{(\rm in,in)}/\sigma_{\rm tot} \approx 0.6$. For comparison $\sigma^{(\rm el,el)}/\sigma_{\rm tot} \approx 0.04$. This means that for the purely exclusive reactions we get $\sigma^{\rm signal}_{pp\to ppX} \lesssim 0.2$ fb. In order to get an experimental value in the fiducial volume $\sigma_{pp\to pp\gamma\gamma} \approx 7$ fb within the $2 \to 1$ approach, often used in the literature, we have to assume a rather large value of $g_{\rm TC} \approx 40$. This is a huge value and puts into doubt the perturbative approach. The corresponding total decay width is $\Gamma_{\rm tot} = 0.16$ GeV (very narrow width). The narrow width approximation was preferred by the CMS analysis [4].

In Fig. 7 we show the $\tilde{\pi}^0$ rapidity distribution. We show here both the contribution of $2 \to 1$ (see Fig. 1) and two contributions of $2 \to 2$ (see Fig. 2) processes. Each of the $2 \to 2$ ($\gamma q \to \tilde{\pi}^0 q$ and $q\gamma \to \tilde{\pi}^0 q$) contributions separately is asymmetric with respect to $y_{\tilde{\pi}^0} = 0$. The sum is then similar as for the $2 \to 1$ contribution. The calculation of rapidity distribution of $\tilde{\pi}^0$ for the mechanism with $2 \to 3$ subprocess (see Fig. 3) is more complicated and will be omitted here.

As discussed in Sec. III C the production of technipion can be calculated also as the $2 \to 3$ subprocess with intermediate (off-shell) photons. Before we shall present corresponding cross section(s) for the $pp \to \tilde{\pi}^0 jj$ reaction we wish to show some interesting results for the partonic $qq' \to q\tilde{\pi}^0 q'$ cross section. When discussing partonic cross section we shall show results for unit electric charges of quarks/antiquarks. The real quark charges are then included in the hadronic cross section. The integrated partonic cross section is an integral over four properly chosen kinematic

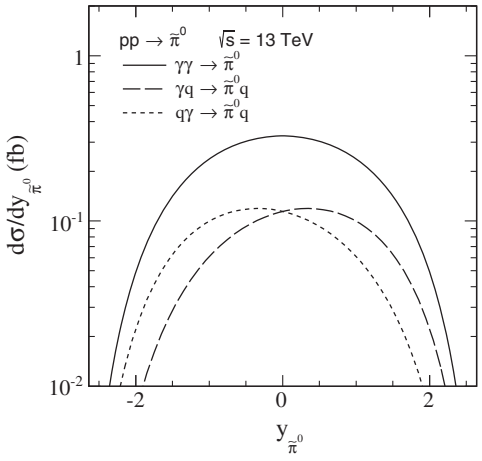

FIG. 7. Distribution in rapidity of neutral technipion for all partonic subprocesses for the $pp \to \tilde{\pi}^0$ at $\sqrt{s} = 13$ TeV. In the calculation we take $g_{\rm TC} = 10$, $m_{\tilde{\pi}^0} = 750$ GeV, $m_q = 1$ MeV (for all flavors), $m_{\tilde{Q}} = 0.75 m_{\tilde{\pi}^0}$ (for both techniflavors).

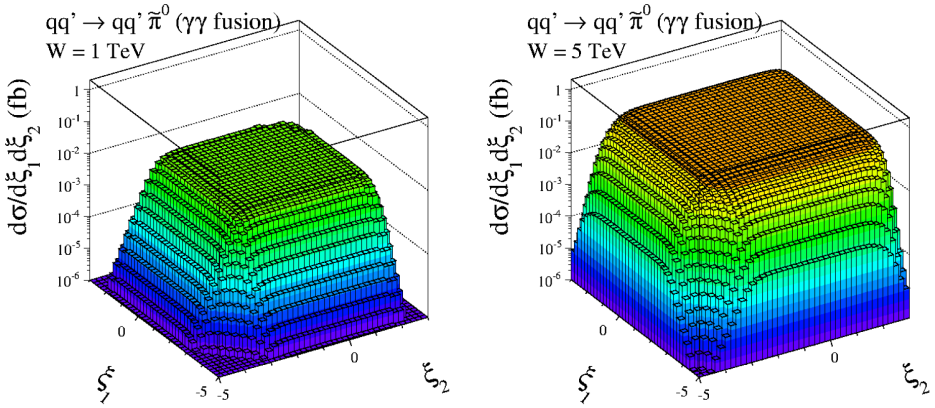

FIG. 8. Differential $qq' \to q\tilde{\pi}^0 q'$ cross section (unit charges) as a function of $\xi_1 = \log_{10}(p_{1t}/1\ \mathrm{GeV})$ and $\xi_2 = \log_{10}(p_{2t}/1\ \mathrm{GeV})$ for two subprocess energies: W = 1 TeV (left panel) and W = 5 TeV (right panel). In this calculation we use $g_{\mathrm{TC}} = 10$ for example.

variables. Different choices are possible *a priori*. In the present calculations we used $\xi_1 = \log_{10}(p_{1t}/1\ \mathrm{GeV})$, $\xi_2 = \log_{10}(p_{2t}/1\ \mathrm{GeV})$, rapidity of technipion and relative azimuthal angle between outgoing quarks/antiquarks. Especially the distribution in ξ_1 and ξ_2 is very interesting and could be even surprising. In Fig. 8 we show the two-dimensional distribution in (ξ_1, ξ_2). The distribution is surprisingly flat over a broad range of ξ_1 and ξ_2 which justifies use of the variables. Here, both very small $p_{1t}, p_{2t} \ll 1$ GeV and very large $p_{1t}, p_{2t} \gg 10$ GeV

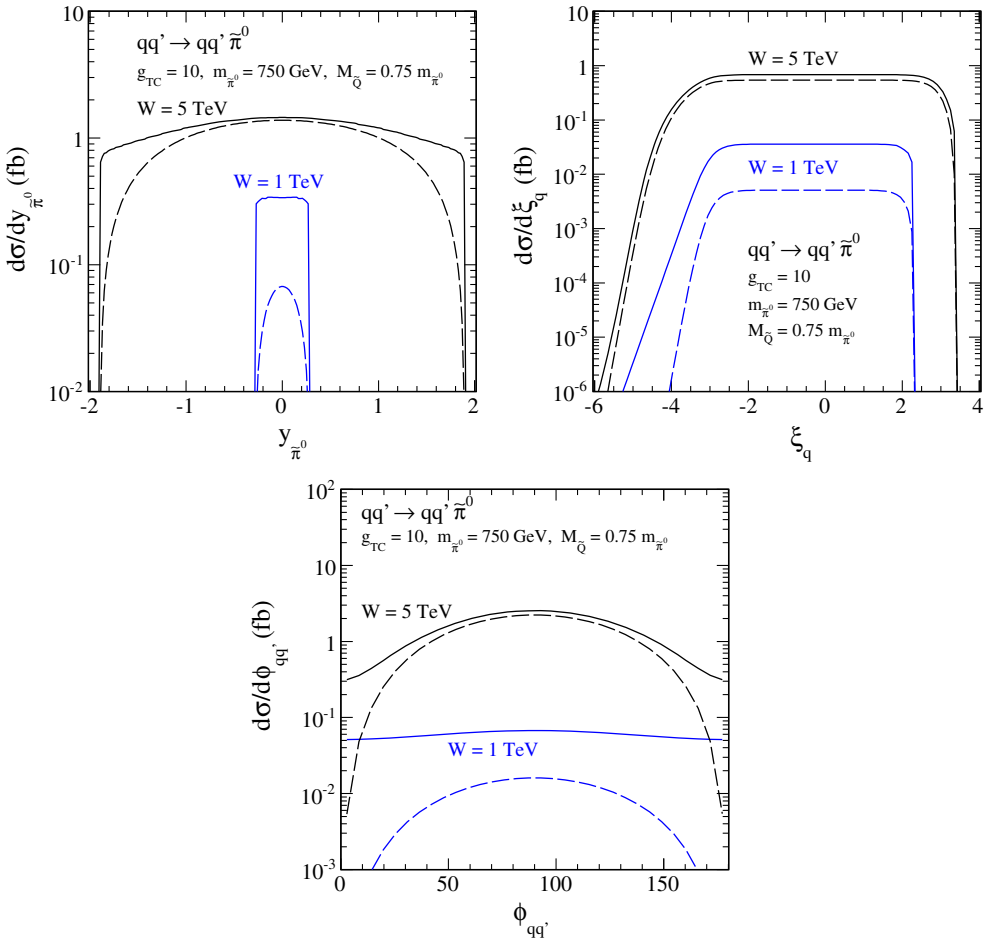

FIG. 9. Differential $qq' \to q\tilde{\pi}^0 q'$ cross sections (assuming unit charges) for two subprocess energies $W = 1$ TeV (blue lower lines) and $W = 5$ TeV (black upper lines). In this calculation we use the set of parameters as shown in the legend. The dashed lines were obtained in the high-energy approximation while the solid lines represent the exact (with spinors) calculations.

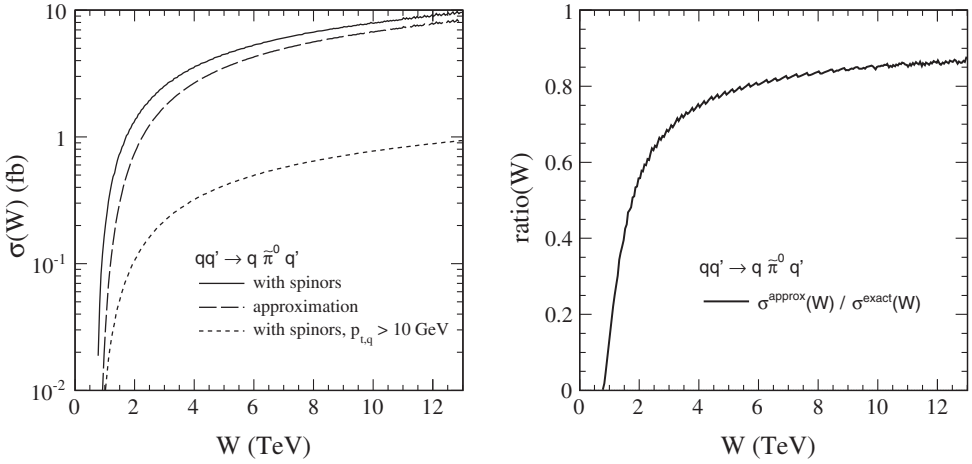

FIG. 10. Left panel: Total partonic $qq' \to q\tilde{\pi}^0 q'$ cross section (unit charges) as a function of subprocess energy. In this calculation $g_{\rm TC} = 10$ was used for example. The solid line is for the calculation with spinors while the dashed line was obtained in the high-energy approximation. The dotted line corresponds to calculation for the exact case with the cut on both transverse momenta of (anti)quarks $p_{1t}, p_{2t} > 10$ GeV. Right panel: Ratio of the total partonic $qq' \to q\tilde{\pi}^0 q'$ cross section (unit charges) in high-energy approximation to the one with spinors as a function of subprocess energy.

transverse momenta of quarks/antiquarks contribute. This would mean that a large fraction of the cross section is associated with one or two jets. We shall return to this point in the conclusion section.

In Fig. 9 we show three different distributions: in rapidity of the technipion, in the integration variable ξ_1 (or ξ_2), and in relative azimuthal angle between the associated "jets." Only some relative azimuthal directions between jets are preferred by the central $\gamma\gamma \to \tilde{\pi}^0$ vertex. These predictions could be also used in searches for technipion associated with one or two jets, which we strongly advocate.

The partonic cross section as a function of subprocess energy W is shown in Fig. 10 (left panel). We observe a quick rise of the cross section from the threshold $W = \sqrt{\hat{s}} = m_{\tilde{\pi}^0}$. In addition to the result with fermions (i.e. including spinors) we show the result for the high-energy approximation often made, e.g. in diffractive processes (see e.g. Ref. [56]). A huge difference between the two results can be observed especially close to the threshold. We show also (dash-dotted line) the cross section when the cut on transverse momenta of (anti)quarks $p_{1t}, p_{2t} > 10$ GeV is imposed in addition. These cross sections are smaller by order of magnitude than the total (without cuts) cross sections but relative background contributions are expected to be smaller. In the right panel of Fig. 10 we show the dependence on subprocess energy of the ratio of the partonic cross section obtained in the high-energy approximation (which coincides with the result for spinless objects) to the one obtained with spinors. At a high subprocess energy the two results start to converge but the energy must be really large in order that the approximation is really good.

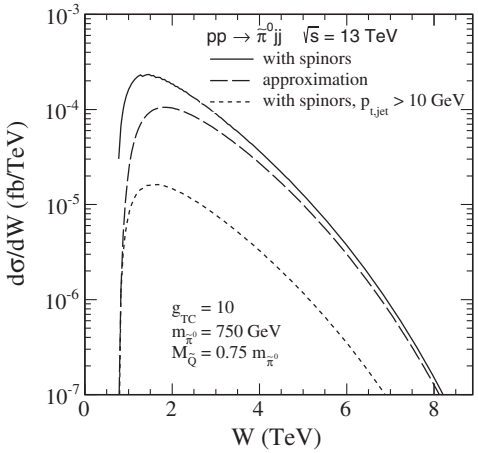

FIG. 11. The distribution in the energy in the partonic subprocess for the $pp \to \tilde{\pi}^0 jj$ at $\sqrt{s} = 13$ TeV. In this calculation we use $g_{\rm TC} = 10$ for example. The solid and dotted lines are for the calculation with spinors while the dashed line was obtained in the high-energy approximation.

Now we proceed to calculations of hadronic cross sections for technipion production. In calculating hadronic cross section we use leading-order MSTW08 parton distributions [57]. In Fig. 11 we show distribution in subsystem energy in proton-proton collision for $\sqrt{s} = 13$ TeV, corresponding to the actual experiments performed by the ATLAS and CMS collaborations. Here we observe that close-to-threshold subenergies are crucial in the calculation. This is the region where the exact (with spinors) and approximate ("spinless quarks") results differ the most.

Performing convolution of the partonic cross section with the quark/antiquark distributions we get for $g_{\rm TC} = 10$: $\sigma = 0.46$ fb for the exact case and $\sigma = 0.24$ fb in the high-energy approximation. Corresponding hadronic cross section with extra cuts on quark transverse momenta

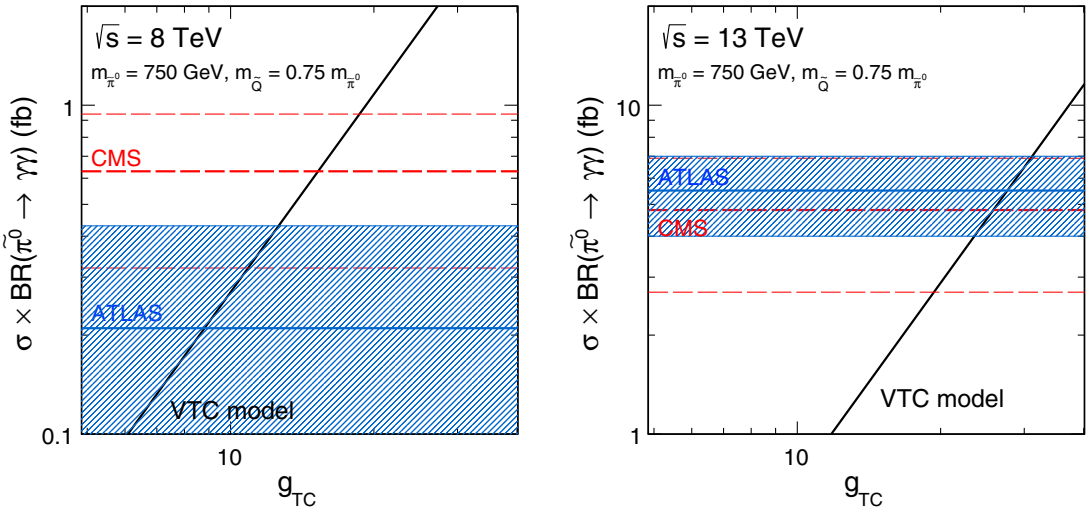

FIG. 12. The dependence of the hadronic $pp \to (\tilde{\pi}^0 \to \gamma\gamma) + X$ cross section on $g_{\rm TC}$ together with the crudely estimated in [58] experimental result at the LHC [3,4]. The solid black line represents our result for the technipion production in the VTC model. The blue shaded band and the red dashed lines represent the experimental uncertainties for ATLAS and CMS measurements, respectively.

$p_{1t}, p_{2t} > 10$ GeV (for the exact case) is 0.04 fb, order of magnitude less than the full phase space one. The cross section for calculation with spinors is only a factor of 2 larger than the one for fictitious spinless quarks, which is often called in the literature high-energy approximation. This is because both small and large $\sqrt{\hat{s}}$ regions enter into the calculation of the hadronic cross section.

The dependence of the cross section on $g_{\rm TC}$ is shown in Fig. 12 for $\sqrt{s} = 8$ TeV (left panel) and $\sqrt{s} = 13$ TeV (right panel) with the experimental uncertainties taken from [58] (narrow width scenario). The model with $g_{\rm TC} = 20$ and $m_{\tilde{Q}} = 0.75 m_{\tilde{\pi}^0}$ is marginally consistent with CMS data, but has difficulty explaining 8 and 13 TeV ATLAS data at the same time. Our result for $g_{\rm TC} = 20$ is at the lower edge of experimental uncertainties at $\sqrt{s} = 13$ TeV and at the upper edge of experimental uncertainties at $\sqrt{s} = 8$ TeV. If $m_{\tilde{Q}}/m_{\tilde{\pi}^0}$ would be smaller the $g_{\rm TC}$ could be lower, see Fig. 8 of [38]. The value of $g_{\rm TC} = 20$ could be also smaller when exchange of Z bosons is included. Inclusion of such mechanisms goes beyond the scope of the present paper and will be done elsewhere.

It is difficult to exclude the discussed model with the current low statistics data. First, because there is a tension between ATLAS and CMS data. Second, there are rather large model uncertainties. As discussed e.g. in [12] the actual energy dependence which is related to x dependence of the photon distributions is rather uncertain. Furthermore, as discussed in our paper there are several contributions to the cross section. Many of them involve elastic or inelastic photon PDFs. In our study here we use one model of photon PDF (MRST-QED [49]). In this model the inelastic-inelastic contribution is (much) bigger than the other three. It is exactly inelastic photon PDF which is so uncertain. Two of us studied the mechanism of photon-photon production of W^+W^- [25] and found large uncertainties related to photon PDFs.

So far the calculation for the 750 GeV object was done using a collinear approximation. There are attempts to include transverse momenta of the photons. First calculations were already done for photon-photon production of dileptons [22,23].

Finally we have included in the moment only processes with "initial" photons. Z bosons should be also taken into consideration in the future.

All this brings model uncertainties difficult to quantify. Only future high statistics data will help to disentangle the situation and answer whether the signal is present at all.

B. Comparison with background contributions

Now we can look at differential distributions and compare the technipion signal to irreducible SM background contributions in the first (photon PDFs) approach. The distributions in rapidity of photons and transverse momentum of one of them $p_{t,\gamma}$ can be calculated in a straightforward way from Eqs. (4.2), (6.1), (6.2), and (6.3). In turn the distribution in diphoton invariant mass can be obtained by an appropriate binning.

Let us consider now two-dimensional distributions for the technipion signal and the $q\bar{q}$ and gg background contributions at $\sqrt{s} = 13$ TeV. In Fig. 13 we show the distributions in photon rapidities limiting to $|y_\gamma| < 2.5$ and in the rapidity and transverse momentum of one of outgoing photons. Our signal obtained in the VTC model strongly contributes at midrapidities $y_\gamma \approx 0$ while the background contributions have a maximum in the regions $(y_{\gamma_1}, y_{\gamma_2}) \approx (\pm 2.5, \mp 2.5)$. The $q\bar{q}$ component of background has on average larger transverse momenta of photons than the gg component. In Fig. 14 we show the

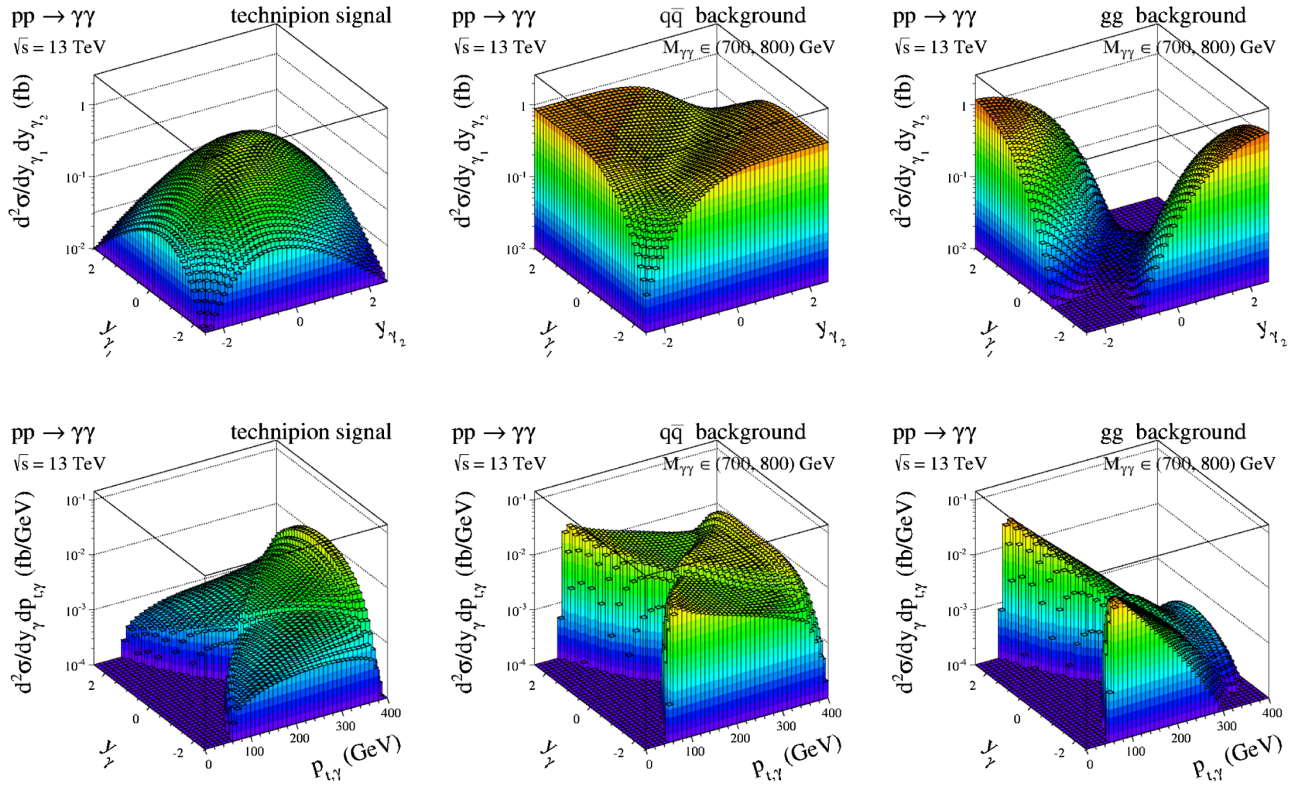

FIG. 13. Two-dimensional distributions in rapidity of photons (top panels) and distributions in photon rapidity and transverse momentum (bottom panels). The signal (technipion) contribution with elastic and inelastic photon fluxes and the background contributions in the diphoton invariant mass range $M_{\gamma\gamma} \in (700, 800)$ GeV are shown. In the technipion calculation $g_{\rm TC} = 20$ was used.

dominant $q\bar{q}$ background contribution with extra limitations on both photon transverse momenta $p_{t,\gamma} > 0.4M_{\gamma\gamma}$ that are inspired by the recent ATLAS analysis at $\sqrt{s} =$ 13 TeV [3]. The experimental cuts $p_{t,\gamma} > 0.4M_{\gamma\gamma}$ significantly decrease the gg and $q\bar{q}$ background cross sections [in the region $M_{\gamma\gamma} \in (700, 800)$ GeV] from $\sigma_{gg} = 4.95$ to 0.17 fb and from $\sigma_{q\bar{q}} = 15.05$ to 5.22 fb, respectively, and lead to a rather small damping for the signal contribution from $\sigma_{\tilde{\pi}^0} = 3.91$ to 2.62 fb.

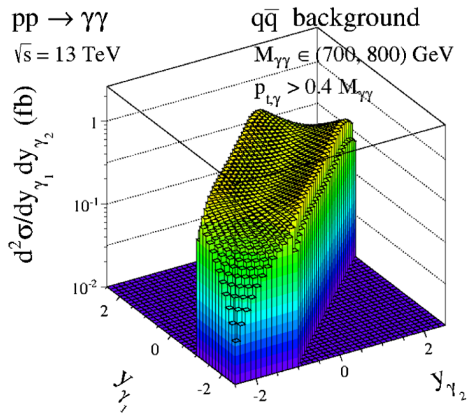

FIG. 14. Two-dimensional distribution for the $q\bar{q}$-annihilation contribution at $\sqrt{s} = 13$ TeV in the diphoton invariant mass range $M_{\gamma\gamma} \in (700, 800)$ GeV with extra limitations on both photon transverse momenta $p_{t,\gamma} > 0.4M_{\gamma\gamma}$.

The most important is the distribution in diphoton invariant mass where the signal was observed by the ATLAS and CMS collaborations. In Fig. 15 we show four examples relevant for different experiments using their kinematic conditions: D0 at $\sqrt{s} = 1.96$ TeV [59], ATLAS at $\sqrt{s} = 7$ TeV [60] (see also CMS data in [61]), ATLAS at $\sqrt{s} = 13$ TeV [3] (see also CMS data in [4]), and the prediction for the Future Circular Collider at $\sqrt{s} = 100$ TeV. We show both signal and background (see the previous section) contributions. Clearly the $q\bar{q}$ annihilation contribution dominates, especially at large invariant masses in the surrounding of the signal. In the photon-induced contributions all components (elastic-elastic, elastic-inelastic, inelastic-inelastic) were taken into account. The $\gamma\gamma$ contribution shows two slopes. For $M_{\gamma\gamma} > 200$ GeV the boxes with the W boson dominate [38]. The experimental smearing effect leads to a significant modification of the sharp peaks, e.g. for the Higgs signal, see Ref. [21]. The experimental invariant mass resolution was included for the signal-technipion calculations in the following simple way:

$$\frac{d\sigma}{dM_{\gamma\gamma}} = \sigma_{\tilde{\pi}^0} \frac{1}{\sqrt{2\pi}\sigma} \exp\left(\frac{-(M_{\gamma\gamma} - m_{\tilde{\pi}^0})^2}{2\sigma^2}\right). \quad (7.1)$$

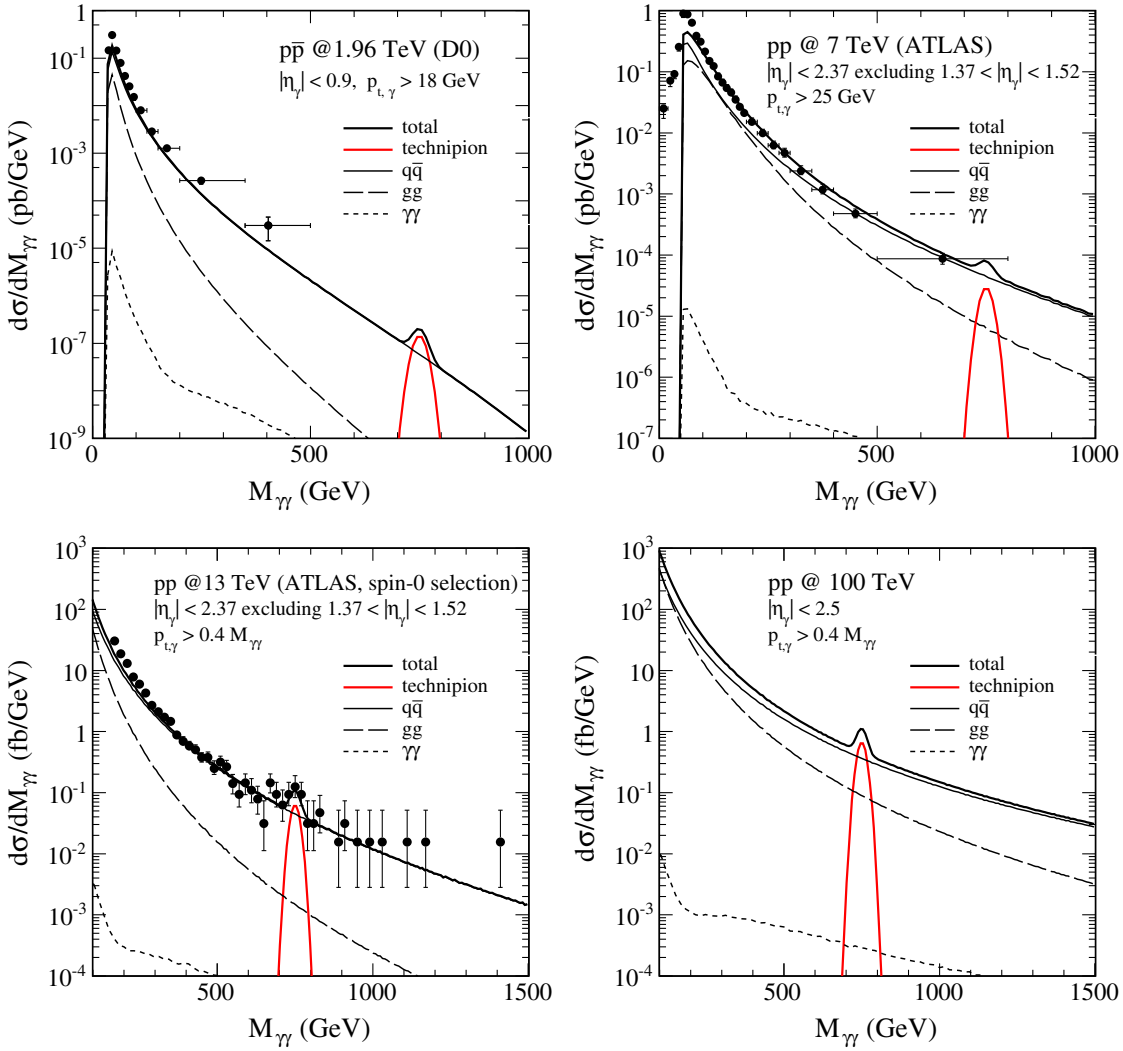

FIG. 15. The two-photon invariant mass distributions for different background contributions and the signal-technipion predictions obtained in the VTC model including experimental cuts. For comparison, the experimental data from D0 [59] at $\sqrt{s} = 1.96$ TeV, ATLAS at $\sqrt{s} = 7$ TeV [60], the recent ATLAS data (spin-0 selection) at $\sqrt{s} = 13$ TeV [3] and our prediction for the Future Circular Collider are presented.

In the calculation we take $\sigma = 15$ GeV assuming $\sigma/m_{\tilde{\pi}^0} \sim 2\%$. In Eq. (7.1) we take $\sigma_{\tilde{\pi}^0} = 0.005$, 1.09, 2.36, and 24.83 fb corresponding to $\sqrt{s} = 1.96$, 7, 13, and 100 TeV, respectively, including the relevant kinematical cuts shown in the panels of Fig. 15. The values of cross sections above were obtained from Eq. (4.2) and $g_{\rm TC} = 20$.

C. Comparison of WTC signal with the existing data for dijets production

Finally in Fig. 16 we show the one-family WTC signal of technipion in the dijet final state together with the CDF [62] and ATLAS [63] data. For a corresponding diagram of the production mechanism see the right panel of Fig. 5. In the case of the ATLAS data we show separate results for different ranges of an auxiliary variable: $y^* = |y_1 - y_2|/2$. In both cases the translated signal is below the experimental data. This means that the model cannot be excluded. Although when the model total (gluon-gluon) decay width of 1.2 GeV [see Eq. (5.1)] was used and experimental resolution was ignored some tension could be probably observed. In an older version of the model [64] (top quark mass solely generated through the extended technicolor approach) also a strong coupling of isoscalar technipion to top quarks was considered, which would lead to a (too) strong signal in the $t\bar{t}$ channel. However, the top quark mass may arise also from other mechanisms like top condensation for instance. In our analysis here we followed therefore the recent version of the model [42], where the coupling to top quarks is totally neglected.

We show also the standard dijet background contribution calculated in leading-order pQCD, which is sufficient for the present precision of searches for the signal of new physics. To improve the precision of the description of the

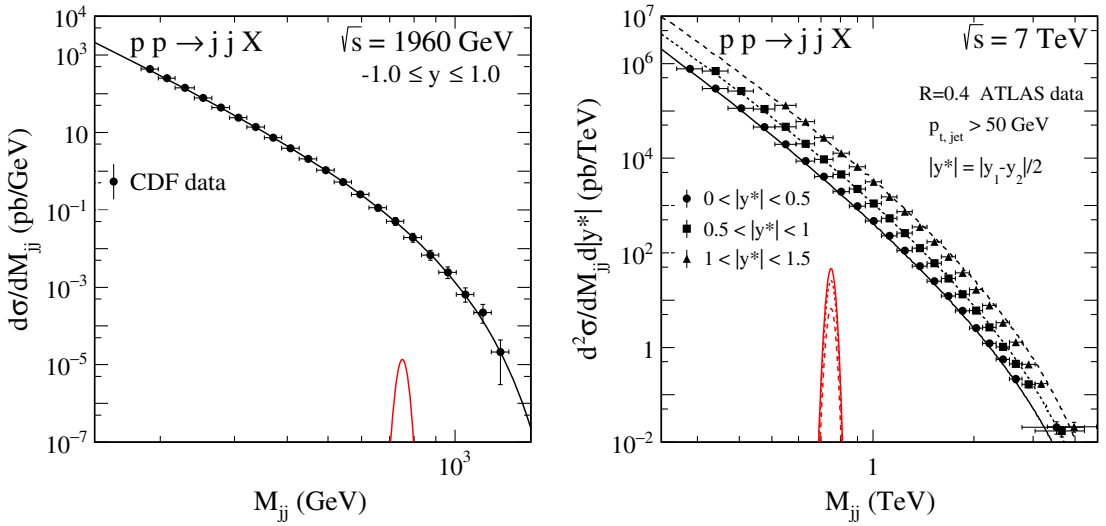

FIG. 16. Dijet invariant mass distribution for the one-family walking technipion (red lines). We show results of both the CDF [62] (left panel) and ATLAS [63] (right panel) collaborations. Please note different order of lines for the signal and the background contributions. In this calculation we use leading-order MSTW08 PDFs [57] and $\mu_F^2 = p_{t,\mathrm{jet}}^2$.

data a K-factor simulating higher-order corrections was applied in the case of the CDF data. In all cases the estimated signal including, similarly as for the diphoton final state, a 2% dijet invariant mass resolution, is substantially below experimental data and standard dijet contribution. We observe a clear tendency that the signal-to-background ratio improves (increases) when going to small values of y^* (please note different ordering of lines for signal and background contributions).

VIII. CONCLUSIONS AND OUTLOOK

In the present paper we have discussed a possibility that diphoton signal at invariant mass $M_{\gamma\gamma} \approx 750$ GeV, recently observed by the ATLAS and CMS collaborations, corresponds to a neutral technipion. The main emphasis has been put on the chirally symmetric (vectorlike) technicolor (VTC) model with two mass degenerate (techni)flavors. In this model only $\gamma\gamma$, γZ and ZZ couplings are possible. Therefore the decay width is rather small $\Gamma_{\mathrm{tot}} \ll 1$ GeV, unless some other decays into stable objects—candidate(s) for dark matter—are considered.

We have discussed in detail the technipion production mechanisms within the VTC model. In the present analysis we have included only photon initiated processes which should be sufficient to estimate parameters of the model. In some modern parton distribution models also photons are included as partons in the proton. In this model there is a rich pattern of electroweak contributions. We have considered $2 \to 1$, $2 \to 2$ and $2 \to 3$ type of subprocesses ($\gamma\gamma \to \tilde{\pi}^0$, $\gamma q \to \tilde{\pi}^0 q$, $qq' \to q\tilde{\pi}^0 q'$) and discussed also some interesting technical details of the calculation. We have found that they give similar contributions to the hadronic cross section. In order to describe the observed "signal" we had to adjust model coupling of techniquarks to the neutral technipion. Including the photon initiated processes we have found $g_{\mathrm{TC}} \simeq 20$, although it is rather difficult to describe all existing CMS and ATLAS experimental data simultaneously. Several differential distributions have been presented for the photon induced processes. Some specific features of the $2 \to 3$ calculations have been illustrated and discussed.

Having adjusted the g_{TC} parameter we have made predictions for the Tevatron, LHC (at $\sqrt{s} = 7$ TeV) and for the Future Circular Collider. The predictions for the Tevatron and ATLAS have been compared with existing data in the diphoton channel. We have concluded that the cross section for energies lower than 8 TeV are so small (below background for integrated luminosity limit) that the signal could not be observed.

We have shown that in order to improve the signal-to-background ratio one could try to measure the hypothetical technipion signal together with one or two jets. With mild cuts (small lower cuts on jet transverse momenta) the cross section is reduced only by not more than 1 order of magnitude. The reduction is of course larger than in the case when we require the presence of two jets. Already the requirement of only one extra jet looks promising. This issue requires further detailed studies, which could be done in the case when the signal is confirmed at the LHC with a better statistics.

We have also made predictions for the purely exclusive case, called here the elastic-elastic case for the sake of brevity. We have predicted that the corresponding cross section should be of the order of 0.2 fb at $\sqrt{s} = 13$ TeV. To focus on such a case one has to measure technipion (two photons) in the central detectors as well as both protons in forward directions. Relevant "forward detectors" are being

installed both by the ATLAS and CMS collaborations. Unfortunately, our predicted cross section seems too small to allow for interesting studies of spin and parity of the resonance discussed very recently [65].

For comparison we have considered also an alternative one-family walking technicolor (WTC) model. In this model gluon-gluon fusion is the dominant production mechanism of the assumed isoscalar technipion. Such an object decays also into the two-gluon (dijet) final state. We have presented predictions of this model for the dijet final state and found the corresponding signal significantly below the CDF and ATLAS data as well as below the standard dijet background. We have found that signal-to-background ratio strongly depends on the so-called y^* variable. The smaller y^* the larger the signal-to-background ratio is. The WTC model could be further verified in the future by considering a four-jet analysis $pp \to (\tilde{\pi}^0 \to jj)jj$ in a similar way as has been done for the VTC model for $pp \to (\tilde{\pi}^0 \to \gamma\gamma)jj$. The background would be then the QCD production of four jets (two forward and two central) which is now calculable for leading and next-to-leading collinear approximation (see, e.g. [66]) as well as in the k_t-factorization approach [67]. This clearly goes beyond the scope of the present paper and will be done elsewhere. In the WTC model the two-jet signal with two extra jets would be reduced by an order of magnitude while the background by at least 2 orders of magnitude.

In summary, neither of the considered technicolor models can be excluded by the present world $\gamma\gamma$ and dijet experimental data. We have shown that the diphoton signal in the VTC model is consistent with all existing diphoton experimental data. The experimental signal for $Z\gamma$ and ZZ (similar production rate as for $\gamma\gamma$ is predicted in the VTC model) is much smaller as it includes branching fraction(s) for the decay of Z boson (s) into e.g. leptons. A combined analysis of different final states (leptons, jets) is required but is of course much more complicated. The WTC model predicts the existence of many states such as isotriplet of states called by the authors P^0, P^+, P^- [68]. They predict the mass of the state(s) at $M \approx 900$ GeV. The neutral member of the triplet could also decay into the $\gamma\gamma$ final state. Due to its quantum numbers it cannot be, however, produced by the gluon-gluon fusion so the corresponding signal would be much weaker than for the isoscalar state discussed in the present paper and therefore difficult to be observed. The isotriplet technirho meson was suggested [69] as a possible explanation of the diboson enhancement observed by the ATLAS collaboration [70,71] at $M \approx 2$ TeV.

In the present paper we have made a consistency analysis of two selected technicolor models as far as technipion production is considered. A similar, rather straightforward, analysis can be made also for axion production. For example for the model considered in Ref. [72], the axion is produced also via photon-photon fusion and the methods discussed here apply.

ACKNOWLEDGMENTS

We are indebted to Wolfgang Schäfer for a discussion on $\gamma\gamma$ induced processes and to Shinya Matsuzaki for explanation of several details of their works on the walking technicolor model. This research was partially supported by the Polish National Science Centre Grants No. DEC-2013/09/D/ST2/03724 and No. DEC-2014/15/B/ST2/02528 and by the Centre for Innovation and Transfer of Natural Sciences and Engineering Knowledge in Rzeszów. R. P. was partially supported by the Swedish Research Council Grant No. 2013-4287.

[1] G. Aad *et al.* (ATLAS Collaboration), Search for resonances decaying to photon pairs in 3.2 fb^{-1} of pp collisions at $\sqrt{s} = 13$ TeV with the ATLAS detector, Report No. ATLAS-CONF-2015-081, 2015.

[2] V. Khachatryan *et al.* (CMS Collaboration), Search for new physics in high mass diphoton events in proton-proton collisions at 13 TeV, Report No. CMS PAS EXO-15-004, 2015.

[3] M. Aaboud *et al.* (ATLAS Collaboration), Search for resonances in diphoton events at $\sqrt{s} = 13$ TeV with the ATLAS detector, arXiv:1606.03833.

[4] V. Khachatryan *et al.* (CMS Collaboration), Search for resonant production of high-mass photon pairs in proton-proton collisions at $\sqrt{s} = 8$ and 13 TeV, arXiv:1606.04093.

[5] G. Aad *et al.* (ATLAS Collaboration), Search for Scalar Diphoton Resonances in the Mass Range 65–600 GeV with the ATLAS Detector in pp Collision Data at $\sqrt{s} = 8$ TeV, Phys. Rev. Lett. **113**, 171801 (2014).

[6] J. Ellis, S. A. R. Ellis, J. Quevillon, V. Sanz, and T. You, On the interpretation of a possible ~750 GeV particle decaying into $\gamma\gamma$, J. High Energy Phys. 03 (2016) 176.

[7] R. Franceschini, G. F. Giudice, J. F. Kamenik, M. McCullough, A. Pomarol, R. Rattazzi, M. Redi, F. Riva, A. Strumia, and R. Torre, What is the $\gamma\gamma$ resonance at 750 GeV?, J. High Energy Phys. 03 (2016) 144.

[8] M. Backovic, A. Mariotti, and D. Redigolo, Diphoton excess illuminates dark matter, J. High Energy Phys. 03 (2016) 157.

[9] S. Di Chiara, L. Marzola, and M. Raidal, First interpretation of the 750 GeV diphoton resonance at the LHC, Phys. Rev. D **93**, 095018 (2016).

[10] C. Csáki, J. Hubisz, and J. Terning, Minimal model of a diphoton resonance: Production without gluon couplings, Phys. Rev. D **93**, 035002 (2016).

[11] C. Csáki, J. Hubisz, S. Lombardo, and J. Terning, Gluon versus photon production of a 750 GeV diphoton resonance, Phys. Rev. D **93**, 095020 (2016).

[12] S. Fichet, G. von Gersdorff, and C. Royon, Scattering light by light at 750 GeV at the LHC, Phys. Rev. D **93**, 075031 (2016).

[13] S. Fichet, G. von Gersdorff, and C. Royon, Measuring the Diphoton Coupling of a 750 GeV Resonance, Phys. Rev. Lett. **116**, 231801 (2016).

[14] F. Staub *et al.*, Precision tools and models to narrow in on the 750 GeV diphoton resonance, arXiv:1602.05581.

[15] L. Bian, N. Chen, D. Liu, and J. Shu, Hidden confining world on the 750 GeV diphoton excess, Phys. Rev. D **93**, 095011 (2016).

[16] A. Ahmed, B. M. Dillon, B. Grzadkowski, J. F. Gunion, and Y. Jiang, Higgs-radion interpretation of 750 GeV diphoton excess at the LHC, arXiv:1512.05771.

[17] B. M. Dillon and V. Sanz, A little KK graviton at 750 GeV, arXiv:1603.09550.

[18] D. B. Franzosi and M. T. Frandsen, Symmetries and composite dynamics for the 750 GeV diphoton excess, arXiv:1601.05357.

[19] M. Łuszczak, R. Maciuła, and A. Szczurek, Subdominant terms in the production of $c\bar{c}$ pairs in proton-proton collisions, Phys. Rev. D **84**, 114018 (2011).

[20] R. Maciuła, R. Pasechnik, and A. Szczurek, Exclusive $b\bar{b}$ pair production and irreducible background to the exclusive Higgs boson production, Phys. Rev. D **82**, 114011 (2010).

[21] R. Maciuła, R. Pasechnik, and A. Szczurek, Central exclusive quark-antiquark dijet and Standard Model Higgs boson production in proton-(anti)proton collisions, Phys. Rev. D **83**, 114034 (2011).

[22] G. G. da Silveira, L. Forthomme, K. Piotrzkowski, W. Schäfer, and A. Szczurek, Central μ^+ μ^- production via photon-photon fusion in proton-proton collisions with proton dissociation, J. High Energy Phys. 02 (2015) 159.

[23] M. Łuszczak, W. Schäfer, and A. Szczurek, Two-photon dilepton production in proton-proton collisions: two alternative approaches, Phys. Rev. D **93**, 074018 (2016).

[24] P. Lebiedowicz, R. Pasechnik, and A. Szczurek, QCD diffractive mechanism of exclusive W^+W^- pair production at high energies, Nucl. Phys. **B867**, 61 (2013).

[25] M. Łuszczak, A. Szczurek, and C. Royon, W^+W^- pair production in proton-proton collisions: Small missing terms, J. High Energy Phys. 02 (2015) 098.

[26] P. Lebiedowicz and A. Szczurek, Exclusive production of heavy charged Higgs boson pairs in the $pp \to ppH^+H^-$ reaction at the LHC and a future circular collider, Phys. Rev. D **91**, 095008 (2015).

[27] S. Weinberg, Implications of dynamical symmetry breaking, Phys. Rev. D **13**, 974 (1976).

[28] L. Susskind, Dynamics of spontaneous symmetry breaking in the Weinberg-Salam theory, Phys. Rev. D **20**, 2619 (1979).

[29] E. Eichten and K. D. Lane, Dynamical breaking of weak interaction symmetries, Phys. Lett. B **90**, 125 (1980).

[30] M. E. Peskin and T. Takeuchi, A New Constraint on a Strongly Interacting Higgs Sector, Phys. Rev. Lett. **65**, 964 (1990).

[31] M. E. Peskin and T. Takeuchi, Estimation of oblique electroweak corrections, Phys. Rev. D **46**, 381 (1992).

[32] J. Galloway, J. A. Evans, M. A. Luty, and R. A. Tacchi, Minimal conformal technicolor and precision electroweak tests, J. High Energy Phys. 10 (2010) 086.

[33] A. Arbey, G. Cacciapaglia, H. Cai, A. Deandrea, S. Le Corre, and F. Sannino, Fundamental composite electroweak dynamics: Status at the LHC, arXiv:1502.04718.

[34] C. T. Hill and E. H. Simmons, Strong dynamics and electroweak symmetry breaking, Phys. Rep. **381**, 235 (2003); **390**, 553(E) (2004).

[35] F. Sannino, Conformal dynamics for TeV physics and cosmology, Acta Phys. Pol. B **40**, 3533 (2009).

[36] C. Kilic, T. Okui, and R. Sundrum, Vectorlike confinement at the LHC, J. High Energy Phys. 02 (2010) 018.

[37] R. Pasechnik, V. Beylin, V. Kuksa, and G. Vereshkov, Chiral-symmetric technicolor with standard model Higgs boson, Phys. Rev. D **88**, 075009 (2013).

[38] P. Lebiedowicz, R. Pasechnik, and A. Szczurek, Search for technipions in exclusive production of diphotons with large invariant masses at the LHC, Nucl. Phys. **B881**, 288 (2014).

[39] R. Pasechnik, V. Beylin, V. Kuksa, and G. Vereshkov, Scalar technibaryon dark matter from vectorlike SU(2) technicolor, Int. J. Mod. Phys. A **31**, 1650036 (2016).

[40] G. Cacciapaglia and F. Sannino, Fundamental composite (Goldstone) Higgs dynamics, J. High Energy Phys. 04 (2014) 111.

[41] A. Hietanen, R. Lewis, C. Pica, and F. Sannino, Fundamental composite Higgs dynamics on the lattice: SU(2) with two flavors, J. High Energy Phys. 07 (2014) 116.

[42] S. Matsuzaki and K. Yamawaki, 750 GeV diphoton signal from one-family walking technipion, Mod. Phys. Lett. A **31**, 1630016 (2016).

[43] E. Molinaro, F. Sannino, and N. Vignaroli, Minimal composite dynamics versus axion origin of the diphoton excess, arXiv:1512.05334.

[44] A. Pilaftsis, Diphoton signatures from heavy axion decays at the CERN Large Hadron Collider, Phys. Rev. D **93**, 015017 (2016).

[45] Y. Mambrini, G. Arcadi, and A. Djouadi, The LHC diphoton resonance and dark matter, Phys. Lett. B **755**, 426 (2016).

[46] N. Tetradis, The quark meson model and the phase diagram of two flavor QCD, Nucl. Phys. **A726**, 93 (2003).

[47] M. Drees and D. Zeppenfeld, Production of supersymmetric particles in elastic ep collisions, Phys. Rev. D **39**, 2536 (1989).

[48] M. Drees, R. M. Godbole, M. Nowakowski, and S. D. Rindani, $\gamma\gamma$ processes at high energy pp colliders, Phys. Rev. D **50**, 2335 (1994).

[49] A. D. Martin, R. G. Roberts, W. J. Stirling, and R. S. Thorne, Parton distributions incorporating QED contributions, Eur. Phys. J. C **39**, 155 (2005).

[50] R. Mertig, M. Bohm, and A. Denner, FEYN CALC: Computer algebraic calculation of Feynman amplitudes, Comput. Phys. Commun. **64**, 345 (1991).

[51] V. Shtabovenko, R. Mertig, and F. Orellana, New developments in FeynCalc 9.0, arXiv:1601.01167.
[52] E. L. Berger, E. Braaten, and R. D. Field, Large-p_T production of single and double photons in proton-proton and pion-proton collisions, Nucl. Phys. **B239**, 52 (1984).
[53] E. W. N. Glover and J. J. van der Bij, Vector boson pair production via gluon fusion, Phys. Lett. B **219**, 488 (1989).
[54] T. Hahn and M. Perez-Victoria, Automatized one loop calculations in four-dimensions and D-dimensions, Comput. Phys. Commun. **118**, 153 (1999).
[55] G. J. van Oldenborgh and J. A. M. Vermaseren, New algorithms for one loop integrals, Z. Phys. C **46**, 425 (1990).
[56] P. Lebiedowicz, O. Nachtmann, and A. Szczurek, Central exclusive diffractive production of the $\pi^+\pi^-$ continuum, scalar and tensor resonances in pp and $p\bar{p}$ scattering within the tensor Pomeron approach, Phys. Rev. D **93**, 054015 (2016).
[57] A. D. Martin, W. J. Stirling, R. S. Thorne, and G. Watt, Parton distributions for the LHC, Eur. Phys. J. C **63**, 189 (2009).
[58] A. Strumia, Interpreting the 750 GeV digamma excess: A review, arXiv:1605.09401, http://inspirehep.net/record/1466435/files/arXiv:1605.09401.pdf.
[59] V. M. Abazov *et al.* (D0 Collaboration), Measurement of the differential cross sections for isolated direct photon pair production in $p\bar{p}$ collisions at $\sqrt{s} = 1.96$ TeV, Phys. Lett. B **725**, 6 (2013).
[60] G. Aad *et al.* (ATLAS Collaboration), Measurement of isolated-photon pair production in pp collisions at $\sqrt{s} = 7$ TeV with the ATLAS detector, J. High Energy Phys. 01 (2013) 086.
[61] S. Chatrchyan *et al.* (CMS Collaboration), Measurement of differential cross sections for the production of a pair of isolated photons in pp collisions at $\sqrt{s} = 7$ TeV, Eur. Phys. J. C **74**, 3129 (2014).
[62] T. Aaltonen *et al.* (CDF Collaboration), Search for new particles decaying into dijets in proton-antiproton collisions at $\sqrt{s} = 1.96$ TeV, Phys. Rev. D **79**, 112002 (2009).
[63] G. Aad *et al.* (ATLAS Collaboration), Measurement of dijet cross sections in pp collisions at 7 TeV center-of-mass energy using the ATLAS detector, J. High Energy Phys. 05 (2014) 059.
[64] J. Jia, S. Matsuzaki, and K. Yamawaki, Walking technipions at the LHC, Phys. Rev. D **87**, 016006 (2013).
[65] L. A. Harland-Lang, V. A. Khoze, and M. G. Ryskin, The production of a diphoton resonance via photon-photon fusion, J. High Energy Phys. 03 (2016) 182.
[66] Z. Bern, G. Diana, L. J. Dixon, F. Febres Cordero, S. Hoeche, D. A. Kosower, H. Ita, D. Maitre, and K. Ozeren, Four-Jet Production at the Large Hadron Collider at Next-to-Leading Order in QCD, Phys. Rev. Lett. **109**, 042001 (2012).
[67] K. Kutak, R. Maciula, M. Serino, A. Szczurek, and A. van Hameren, Four-jet production in single- and double-parton scattering within high-energy factorization, J. High Energy Phys. 04 (2016) 175.
[68] M. Kurachi, S. Matsuzaki, and K. Yamawaki, Walking technipions in a holographic model, Phys. Rev. D **90**, 095013 (2014).
[69] H. S. Fukano, M. Kurachi, S. Matsuzaki, K. Terashi, and K. Yamawaki, 2 TeV walking technirho at LHC?, Phys. Lett. B **750**, 259 (2015).
[70] G. Aad *et al.* (ATLAS Collaboration), Search for high-mass diboson resonances with boson-tagged jets in proton-proton collisions at $\sqrt{s} = 8$ TeV with the ATLAS detector, J. High Energy Phys. 12 (2015) 055.
[71] G. Aad *et al.* (ATLAS Collaboration), Combination of searches for WW, WZ, and ZZ resonances in pp collisions at $\sqrt{s} = 8$ TeV with the ATLAS detector, Phys. Lett. B **755**, 285 (2016).
[72] N. D. Barrie, A. Kobakhidze, M. Talia, and L. Wu, 750 GeV composite axion as the LHC diphoton resonance, Phys. Lett. B **755**, 343 (2016).